Probing the Higgs self-coupling at hadron colliders using rare decays

U. Baur*
Department of Physics, State University of New York, Buffalo, New York 14260, USA

T. Plehn†
CERN Theory Group, CH-1211 Geneva 23, Switzerland

D. Rainwater‡
DESY Theorie, Notkestrasse 85, D-22603 Hamburg, Germany

(Received 3 October 2003; published 16 March 2004)

We investigate Higgs boson pair production at hadron colliders for Higgs boson masses $m_H \leqslant 140$ GeV and the rare decay of one of the two Higgs bosons. While in the standard model the number of events is quite low at the CERN Large Hadron Collider (LHC), a first, albeit not very precise, measurement of the Higgs boson self-coupling is possible in the $gg \to HH \to b\bar{b}\gamma\gamma$ channel. A luminosity-upgraded LHC could improve this measurement considerably. A 200 TeV very large hadron collider could make a measurement of the Higgs self-coupling competitive with a next-generation linear collider. In the minimal supersymmetric standard model (MSSM) we find a significant region with observable Higgs boson pair production in the small $\tan\beta$ regime, where resonant production of two light Higgs bosons might be the only hint at the LHC of a MSSM Higgs sector.

DOI: 10.1103/PhysRevD.69.053004 PACS number(s): 14.80.Bn, 13.85.Qk

I. INTRODUCTION

The CERN Large Hadron Collider (LHC) is scheduled to begin operation in 2007, beginning a new era wherein the mechanism of electroweak symmetry breaking and fermion mass generation will be revealed and studied in great detail. Although alternative mechanisms exist in theory, this is generally believed to be a light Higgs boson with a mass $m_H < 219$ GeV [1]. More specifically, we expect a fundamental scalar sector which undergoes spontaneous symmetry breaking as the result of a potential which acquires a nonzero vacuum expectation value. The LHC will easily find a light standard model (SM) Higgs boson with a very moderate luminosity [2,3]. Moreover, the LHC will have significant capability to determine many of its properties [4,5], such as its fermionic and bosonic decay modes and couplings [6–9], including invisible decays [10] and possibly even rare decays to second generation fermions [11].[1]

Starting from the requirement that the Higgs boson has to restore unitarity of weak boson scattering at high energies in the SM [13], perhaps the most important measurement after a Higgs boson discovery is of the Higgs potential itself, which requires measurement of the trilinear and quartic Higgs boson self-couplings. Only multiple Higgs boson production can probe these directly [14,15].

Recent literature is replete with self-coupling measurement studies. There are numerous quantitative sensitivity limit analyses of Higgs boson pair production in e^+e^- collisions ranging from 500 GeV to 3 TeV center of mass energies [15–18]. For example, one neural-net-based study concludes that a 500 GeV linear collider with an integrated luminosity of 1 ab^{-1} [18] could measure the trilinear Higgs boson coupling λ for $m_H = 120$ GeV, where $H \to b\bar{b}$ decays dominate, at the 20% level. However, none of these analyses addressed the case of $m_H > 140$ GeV, where the Higgs boson mostly decays into W bosons. Studies exploring the potential of the LHC, a luminosity-upgraded LHC (SLHC) with roughly ten times the amount of data expected in the first run, and a very large hadron collider (VLHC), have come only very recently [19–22]. These studies investigated Higgs boson pair production via gluon fusion with subsequent decay to same-sign dileptons and three leptons via W bosons, and cover the broader range $115 < m_H < 200$ GeV. They established that future hadron machines can probe the Higgs potential for $m_H \gtrsim 150$ GeV. At the LHC, an integrated luminosity of 300 fb^{-1} provides for exclusion of vanishing λ at the 95% confidence level or better over the entire range $150 < m_H < 200$ GeV. A VLHC would provide for precision measurements over much of this mass range, similar to or better than the limits achievable at a 3 TeV e^+e^- collider with 5 ab^{-1} [17]. However, we previously concluded that hadron colliders could not probe the mass region $m_H < 140$ GeV sufficiently well to be meaningful [22].

We reexamine that conclusion in this paper, utilizing rare decay modes in Higgs boson pair production for $m_H < 140$ GeV at future hadron colliders. We first review the definition of the Higgs boson self-couplings and briefly discuss SM and non-SM predictions for these parameters in Sec. II. An overview of the rare Higgs boson decay modes in the SM (predominantly $b\bar{b}\gamma\gamma$ final states) and our analyses

*Email address: baur@ubhex.physics.buffalo.edu
†Email address: tilman.plehn@cern.ch
‡Email address: david.rainwater@desy.de

[1] An e^+e^- linear collider with a center of mass energy of 350 GeV or more can significantly improve these preliminary measurements, in some cases by an order of magnitude in precision, if an integrated luminosity of 500 fb^{-1} can be achieved [12].

of these channels appear in Sec. III. We consider the LHC, SLHC, and a VLHC, which we assume to be a pp collider operating at 200 TeV with a luminosity of $\mathcal{L}=2\times10^{34}\,\mathrm{cm}^{-2}\,\mathrm{s}^{-1}$ [23]. In Sec. IV we establish the prospects of observing a pair of minimal supersymmetric standard model (MSSM) Higgs bosons in the $b\bar{b}\gamma\gamma$ and $b\bar{b}\mu^+\mu^-$ decay channels. We present our conclusions in Sec. V.

II. HIGGS BOSON SELF-COUPLINGS

The trilinear and quartic Higgs boson couplings λ and $\tilde{\lambda}$ are defined through the potential

$$V(\eta_H)=\frac{1}{2}m_H^2\eta_H^2+\lambda v\,\eta_H^3+\frac{1}{4}\tilde{\lambda}\,\eta_H^4, \tag{1}$$

where η_H is the physical Higgs field, $v=(\sqrt{2}G_F)^{-1/2}$ is the vacuum expectation value, and G_F is the Fermi constant. In the SM the self-couplings are

$$\tilde{\lambda}=\lambda=\lambda_{SM}=\frac{m_H^2}{2v^2}. \tag{2}$$

Regarding the SM as an effective theory, the Higgs boson self-couplings λ and $\tilde{\lambda}$ are *per se* free parameters, and S-matrix unitarity constrains $\tilde{\lambda}$ to $\tilde{\lambda}\leqslant 8\pi/3$ [13]. Since future collider experiments likely cannot probe $\tilde{\lambda}$, we concentrate on the trilinear coupling λ in the following. The quartic Higgs boson coupling does not affect the Higgs boson pair production processes we consider.

In the SM, radiative corrections decrease λ by 4–11 % for $120<m_H<200$ GeV [24]. Larger deviations are possible in scenarios beyond the SM. For example, in two Higgs doublet models where the lightest Higgs boson is forced to have SM-like couplings to vector bosons, quantum corrections may increase the trilinear Higgs boson coupling by up to 100% [24]. In the MSSM, loop corrections modify the self-coupling of the lightest Higgs boson in the decoupling limit, which has SM-like couplings, by up to 8% for light stop squarks [25]. Anomalous Higgs boson self-couplings also appear in various other scenarios beyond the SM, such as models with a composite Higgs boson [26], or in little Higgs boson models [27]. In many cases, the anomalous Higgs boson self-couplings can be parametrized in terms of higher dimensional operators which are induced by integrating out heavy degrees of freedom. A systematic analysis of Higgs boson self-couplings in a higher dimensional operator approach can be found in Ref. [28].

III. ANALYSIS

At LHC energies, inclusive Higgs boson pair production is dominated by gluon fusion [29]. Other processes, such as weak boson fusion, $qq\to qqHH$ [30], associated production with heavy gauge bosons, $q\bar{q}\to WHH,ZHH$ [31], or associated production with top quark pairs, $gg,q\bar{q}\to t\bar{t}HH$ [19], yield cross sections which are factors of 10–30 smaller than that for $gg\to HH$ [29]. Since HH production at the LHC is generally rate limited, we consider only the gluon fusion process.

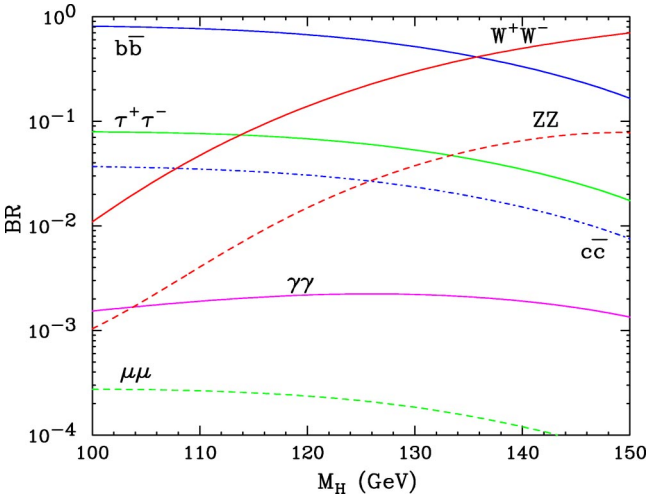

FIG. 1. SM Higgs boson branching ratios relevant to our analysis of HH production. For W^+W^- and ZZ, one of the gauge bosons is off shell.

Because the total $gg\to HH$ cross section at both the LHC and VLHC is quite small, at most one Higgs boson undergoing rare decay will allow for a reasonable number of events to work with. We therefore consider only final states containing one b-quark pair, which is the dominant SM Higgs boson decay mode for $m_H<135$ GeV, as shown in Fig. 1. Our previous study demonstrated that at both the LHC and VLHC $4b$ and $b\bar{b}\tau^+\tau^-$ final states are overwhelmed by background [22]. While the backgrounds are more moderate for the τ channel, the observable part of this decay mode unfortunately has multiple additional small branching ratios, and the detectors have rather low efficiency to identify the τ leptons. As charm quarks are even more difficult to tag than b quarks, and the QCD backgrounds become much larger due to similarly less fake-tag rejection, we can immediately discount any colored final states for the rare decay. Weak boson pairs certainly qualify as rare decays in this mass region, but cannot be used: the $b\bar{b}W^*W$ and $b\bar{b}Z^*Z\to b\bar{b}\ell^+\ell^-\bar{\nu}\nu$ final states suffer from a huge QCD top pair background. Similarly for $pp\to HH\to b\bar{b}Z^*Z$ with one or more hadronically decaying Z bosons, and $b\bar{b}Z\gamma\to b\bar{b}jj\gamma$, QCD processes with the same final states are likely to overwhelm the signal (here, W^* and Z^* denote off-shell W and Z bosons). The $b\bar{b}Z^*Z\to b\bar{b}+4$ leptons and $b\bar{b}Z\gamma\to\ell^+\ell^-\gamma$ channels suffer from too low a rate, due to the small $Z\to\ell^+\ell^-$ branching ratio. This leaves only the diphoton $b\bar{b}\gamma\gamma$ and dimuon $b\bar{b}\mu^+\mu^-$ decay combinations.

For all our calculations we assume an integrated luminosity of 600 fb^{-1} for the LHC, and 6000 fb^{-1} [19] for the SLHC. For the VLHC, we consider both 600 fb^{-1} and 1200 fb^{-1} [23]. We choose $\alpha_s(M_Z)=0.1185$ [32], calculate signal and background cross sections using CTEQ5L [33] parton distribution functions, and our scale choice for all background processes is $\mu_F=\mu_R=\sqrt{\hat{s}}$. We include minimal detector effects by Gaussian smearing of the parton momenta

according to ATLAS expectations [4], and take into account energy loss in the b jets via a parametrized function. We assume a b tagging efficiency of $\epsilon_b = 50\%$ for all hadron colliders. In addition, we include an efficiency of 79% [34] for capturing the $H \to b\bar{b}$ decay of the signal in its 40 GeV mass bin. We calculate all background processes using MADGRAPH [35] except where otherwise noted, and retain a finite b- (c)-quark mass of 4.6 (1.7) GeV where relevant. Other detector efficiencies are given in the subsections relevant to the respective channels.

A. The $b\bar{b}\gamma\gamma$ decay channel

We perform the signal calculation, $gg \to HH \to b\bar{b}\gamma\gamma$, as in Refs. [20,22], including the effects of next-to-leading order (NLO) QCD corrections via a multiplicative factor $K = 1.65$ (1.35) at LHC (VLHC) energies [36], using factorization and renormalization scale choices of m_H. There is little scale variation left at NLO. We use exact matrix elements to incorporate the $H \to b\bar{b}$ and $H \to \gamma\gamma$ decays.

The basic kinematic acceptance cuts for events at the (S)LHC and VLHC are

$$p_T(b) > 45 \text{ GeV}, \quad |\eta(b)| < 2.5, \quad \Delta R(b,b) > 0.4,$$

$$m_H - 20 \text{ GeV} < m_{b\bar{b}} < m_H + 20 \text{ GeV},$$

$$p_T(\gamma) > 20 \text{ GeV}, \quad |\eta(\gamma)| < 2.5, \quad \Delta R(\gamma,\gamma) > 0.4,$$

$$m_H - 2.3 \text{ GeV} < m_{\gamma\gamma} < m_H + 2.3 \text{ GeV},$$

$$\Delta R(\gamma,b) > 0.4, \tag{3}$$

which are motivated first by the requirements that the events can pass the ATLAS and CMS triggers with high efficiency [4,5], and that the b-quark and photon pairs reconstruct to windows around the known Higgs boson mass, adjusted for an expected capture efficiency of 79% each [34]. We take the identification efficiency for each photon to be 80% at all machines considered [34].

As in the $4W$ signal case [20], we will later try to determine the Higgs boson self-coupling from the shape of the invariant mass of the final state. For that reason we do not apply any cuts which make use of the fact that the signal involves two heavy massive particles produced in a fairly narrow range of the $b\bar{b}\gamma\gamma$ invariant mass. The only irreducible background processes are QCD $b\bar{b}\gamma\gamma$, $H(\to\gamma\gamma)b\bar{b}$, and $H(\to b\bar{b})\gamma\gamma$ production. However, there are multiple QCD reducible backgrounds resulting from jets faking either b jets or photons: $c\bar{c}\gamma\gamma$, one or two fake b jets; $b\bar{b}j\gamma$, one fake photon; $c\bar{c}j\gamma$, one or two fake b jets, one fake photon; $jj\gamma\gamma$, one or two fake b jets; $b\bar{b}jj$, two fake photons; $c\bar{c}jj$, one or two fake b jets, two fake photons; $jjj\gamma$, one or two fake b jets, one fake photon; $jjjj$, one or two fake b jets, two fake photons; Hjj, one or two fake b jets, or two fake photons; and $Hj\gamma$, one fake photon.

TABLE I. Expected photon and muon identification efficiencies and misidentification probabilities for charm quarks and light jets as b quarks [4,5,19,37] and photons [4,5,38,39], at various hadron colliders.

	ϵ_γ	ϵ_μ	$P_{c\to b}$	$P_{j\to b}$	$P^{hi}_{j\to\gamma}$	$P^{lo}_{j\to\gamma}$
LHC	80%	90%	1/13	1/140	1/1600	1/2500
SLHC	80%	90%	1/13	1/23	1/1600	1/2500
VLHC	80%	90%	1/13	1/140	1/1600	1/2500

Misidentified charm quarks must be considered separately from nonheavy flavor jets because of the grossly different rejection factors. Table I summarizes the expected rejection factors for charm and light jets to be misidentified as b jets and photons, as well as the expected photon and muon identification efficiencies. The probability of misidentifying a light jet as a b jet is significantly higher at the SLHC due to the high luminosity environment [19]. The value quoted in Table I for $P_{j\to b}$ at the LHC is likely to be conservative; recent studies [37] using three-dimensional b tagging have found a light jet rejection factor about a factor of 2 better. Expectations for the probability of misidentifying a light jet as a photon at the LHC vary considerably [4,5,38,39], so we perform two analyses, one conservative and the other optimistic, to cover this range. Since their design luminosities are similar, it is reasonable to assume that the rejection factors for light quarks and charm quarks, and the jet-photon misidentification probabilities, are similar for the LHC and the VLHC. Studies of how the high luminosity environment of the SLHC affects $P_{c\to b}$ and $P_{j\to\gamma}$ have not yet been performed. In lieu of better estimates we therefore use the same values as for the LHC and VLHC. It should be noted that the rejection factors listed in Table I depend on the transverse momentum of the charm quark, $p_T(c)$, or jet, $p_T(j)$. The values listed in the table correspond to the rejection factor in the p_T range that provides the largest contribution to the cross section.

Except for the $b\bar{b}j\gamma$ and $b\bar{b}jj$ backgrounds, all reducible backgrounds depend on whether one requires one or both b quarks to be tagged. Requiring only one tagged b quark results in a signal cross section that is a factor of $(2/\epsilon_b - 1) = 3$ larger than the one with both b quarks tagged. This larger signal rate comes at the expense of a significantly increased reducible background. As we shall demonstrate, the small $gg \to HH \to b\bar{b}\gamma\gamma$ cross section forces us to require a single b tag at the LHC in order to have an observable signal. At the SLHC, on the other hand, the much higher probability of misidentifying a light jet as a b jet translates into an increase of the background which more than compensates the signal gain from using only a single b tag. In the following we therefore require a double b tag at the SLHC. For the VLHC we consider both single and double b tagging.

For a single b tag strategy, there is an additional combinatorial background when extra jets are present in the event. To estimate this background, one needs to interface the $gg \to HH$ matrix elements with an event generator. Insight may also be gained from performing a calculation of HHj production, which presently does not exist. Since we calculate the

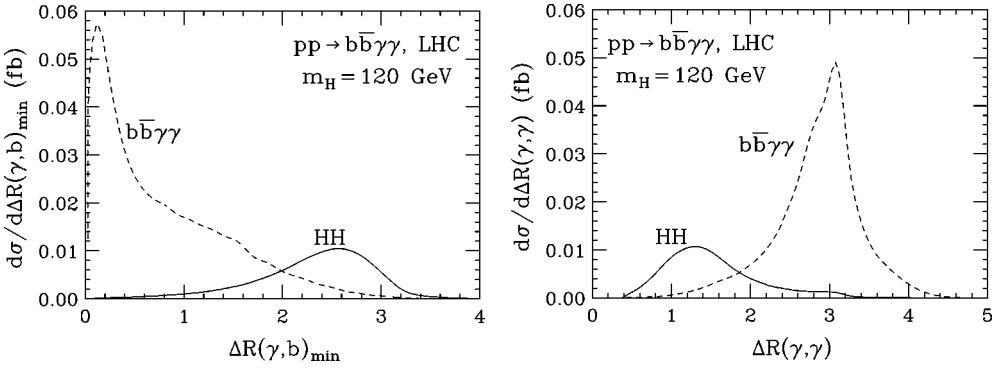

FIG. 2. Distributions of the minimum lego plot (pseudorapidity–transverse plane) separation between (a) b jets and photons, and (b) photons, for a SM signal of $m_H=120$ GeV and the QCD $b\bar{b}\gamma\gamma$ background; using the cuts of Eq. (3) but no minimum b-γ separation. We include the NLO K factor for the signal and a factor of 1.3 for the QCD background.

signal cross section with cuts only at lowest order, we do not include the combinatorial background in our background estimate.

At the level of cuts in Eq. (3), we observe two angular correlations which differ strongly between signal and background. The minimum separation between b jets and photons is typically much smaller for the QCD backgrounds as compared to the signal. The shape of the signal distribution reflects the fact that the $b\bar{b}$ and $\gamma\gamma$ pairs originate from decays of heavy scalar particles which recoil against each other in the transverse plane. The peak in the background $\Delta R(\gamma,b)_{min}$ distribution at small values is clearly due to the collinear enhancement from photon radiation off a b quark. The minimum separation between the photons, on the other hand, is smaller for the signal. We show the minimum photon-b and the photon-photon separation distributions in Fig. 2, for the HH signal and the $b\bar{b}\gamma\gamma$ background at the LHC; all other background processes exhibit distributions qualitatively similar to those for QCD $b\bar{b}\gamma\gamma$ production. Based on these observations, we impose two additional angular cuts on the final state, which reduce the backgrounds by about an order of magnitude, but affect the signal at only the 15–20 % level for $m_H=120$ GeV, and closer to 30% for $m_H=140$ GeV:

$$\Delta R(\gamma,b)>1.0, \quad \Delta R(\gamma,\gamma)<2.0. \tag{4}$$

Looking at Fig. 2, these do not appear to be the optimum values. However, the cuts are correlated, and we chose these values to roughly optimize the signal-to-background ratio (S/B) while retaining a significant fraction of the signal.

Tables II and III display the signal and QCD background cross sections for the (S)LHC and VLHC, including the signal K factor, at the level of cuts in Eq. (3), adding Eq. (4), and finally with all efficiencies and misidentification probabilities applied, for both the conservative ("hi," $P_{j\to\gamma}$

TABLE II. Expected cross sections (fb) (first three rows) for the $m_H=120$ GeV $HH\to b\bar{b}\gamma\gamma$ signal and QCD backgrounds, including the signal K factors, at the (S)LHC. The background cross sections are scaled by a factor of 1.3, as explained in the text. The QCD backgrounds cannot be calculated without cuts due to soft and collinear singularities. Each of the next four pairs of rows shows the cross sections including all detector efficiencies and fake-tag rejection probabilities as described in the text, and the number of events expected, for each machine and background analysis. We assume an integrated luminosity of 600 fb^{-1} (6000 fb^{-1}) for the LHC (SLHC). The Hjj, $Hb\bar{b}$, $H\gamma\gamma$, and $Hj\gamma$ backgrounds are discussed in the text and therefore not shown.

Analysis stage	HH	$b\bar{b}\gamma\gamma$	$c\bar{c}\gamma\gamma$	$b\bar{b}\gamma j$	$c\bar{c}\gamma j$	$jj\gamma\gamma$	$b\bar{b}jj$	$c\bar{c}jj$	γjjj	$jjjj$	Σ(backgrounds)
Before cuts	0.15	—	—	—	—	—	—	—	—	—	—
+ Eq. (3)	0.043	0.056	0.42	65	250	11	2.5×10^4	2.5×10^4	7700	5×10^6	5×10^6
+ Eq. (4)	0.035	0.0060	0.0215	8.28	17.0	0.84	4520	4520	364	4×10^5	4×10^5
$\times\ \epsilon\cdot P^{hi}_{LHC}$	0.0106	0.0029	0.0020	0.0031	0.0013	0.0077	0.0013	0.0003	0.0030	0.0022	0.0233
N_{LHC}(hi)	6	2	1	2	1	5	1	0	2	1	14
$\times\ \epsilon\cdot P^{lo}_{LHC}$	0.0106	0.0029	0.0020	0.0020	0.0008	0.0077	0.0005	0.0001	0.0017	0.0009	0.0186
N_{LHC}(lo)	6	2	1	1	0	5	0	0	1	1	11
$\times\ \epsilon\cdot P^{hi}_{SLHC}$	0.0035	0.0010	0.0001	0.0010	0.0001	0.0010	0.0004	0.0000	0.0003	0.0003	0.0042
N_{SLHC}(hi)	21	6	0	6	0	6	3	0	2	2	25
$\times\ \epsilon\cdot P^{lo}_{SLHC}$	0.0035	0.0010	0.0001	0.0007	0.0000	0.0010	0.0002	0.0000	0.0002	0.0001	0.0033
N_{SLHC}(lo)	21	6	0	4	0	6	1	0	1	1	20

TABLE III. Expected cross sections (fb) (first three rows) for the $m_H = 120$ GeV $HH \to b\bar{b}\gamma\gamma$ signal and QCD backgrounds, including the signal K factors, at the VLHC. The background cross sections are scaled by a factor of 1.3, as explained in the text. The QCD backgrounds cannot be calculated without cuts due to soft and collinear singularities. Each of the next pairs of rows shows the cross sections including all detector efficiencies and fake-tag rejection probabilities as described in the text, and the number of events expected for an integrated luminosity of 600 fb^{-1}, for each of the two background analyses. We show results for both single and double b tagging. The Hjj, $Hb\bar{b}$, $H\gamma\gamma$, and $Hj\gamma$ backgrounds are discussed in the text and therefore not shown.

Analysis stage	HH	$b\bar{b}\gamma\gamma$	$c\bar{c}\gamma\gamma$	$b\bar{b}\gamma j$	$c\bar{c}\gamma j$	$jj\gamma\gamma$	$b\bar{b}jj$	$c\bar{c}jj$	γjjj	$jjjj$	Σ(backgrounds)
Before cuts	15.9	—	—	—	—	—	—	—	—	—	—
+ Eq. (3)	3.12	1.8	23	3600	14000	280	1.6×10^6	1.6×10^6	2.3×10^5	2.7×10^8	2.7×10^8
+ Eq. (4)	2.70	0.14	1.23	417	1020	25.0	4.2×10^5	4.2×10^5	13300	3.0×10^7	3.0×10^7
1 b tag											
$\times\ \epsilon\cdot P^{hi}_{VLHC}$	0.810	0.067	0.116	0.156	0.075	0.228	0.122	0.024	0.095	0.164	1.048
N(hi)	486	40	70	94	45	137	73	14	57	98	629
$\times\ \epsilon\cdot P^{lo}_{VLHC}$	0.810	0.067	0.116	0.100	0.048	0.228	0.050	0.010	0.061	0.067	0.747
N(lo)	486	40	70	60	29	137	30	6	36	40	448
2 b tags											
$\times\ \epsilon\cdot P^{hi}_{VLHC}$	0.270	0.022	0.005	0.052	0.003	0.001	0.041	0.001	0.000	0.001	0.126
N(hi)	162	13	3	31	2	0	25	1	0	1	76
$\times\ \epsilon\cdot P^{lo}_{VLHC}$	0.270	0.022	0.005	0.033	0.002	0.001	0.017	0.000	0.000	0.000	0.080
N(lo)	162	13	3	20	1	0	10	0	0	0	47

$=1/1600$) and optimistic ("lo," $P_{j\to\gamma}=1/2500$) assumptions. The QCD background normalization uncertainty is rather large at LO, and unfortunately none of these processes is known at NLO. To estimate the effect of a possible NLO increase of the background rates, we scale each of the background cross sections by a factor of 1.3. Note that we are not making any statement about unknown higher order corrections. Instead, we attempt to be conservative and show that our results do not critically depend on the background normalization.

Before final state identification, the $\mathcal{O}(\alpha_s^4)$ $jjjj$ background dominates over all others by two orders of magnitude. The angular cuts of Eq. (4) do improve the signal-to-background ratio by an order of magnitude, but it is the cumulative effect of large rejection factors for misidentifying light jets as photons or b jets that brings the QCD backgrounds down to a manageable level.

The single Higgs boson resonance backgrounds are for the most part negligible, so we do not include them in Tables II and III. The Hjj cross section is approximately a factor of 6–20 smaller than the signal [40]; the $Hb\bar{b}$ cross section is a factor of 20–60 smaller. Although no calculations of $H\gamma\gamma$ and $Hj\gamma$ production exist yet, one expects that these backgrounds are also negligible. All subsequent numerical results include the Hjj background, whereas we neglect the $Hb\bar{b}$, $H\gamma\gamma$, and $Hj\gamma$ backgrounds.

Summing all background cross sections we find that $S/B \sim 1/1$ is possible at the SLHC, and we anticipate a still respectable $S/B \sim 1/2$ at the LHC. At the VLHC, with one tagged b quark, we obtain a signal-to-background ratio of about 1/1, while a double b tag yields $S/B \approx 2$–3.5. Of course, even small changes in expected fake-b rejection factors could change how the analysis would be optimized. Our results are meant only to highlight the potential capability of such a search.

Our estimates also reveal that the range of fake-photon rejection probabilities is not so significant. The largest background in most cases is $jj\gamma\gamma$, where the photons are real but one or two b tags are falsely identified—at the SLHC the double b tag requirement brings this background to the same level as the real $b\bar{b}\gamma\gamma$ component. The irreducible $b\bar{b}\gamma\gamma$ background in all cases constitutes only a small fraction of the total background.

As shown in Table III, requiring two b tags instead of one at the VLHC reduces the overall background by a factor of 8–9, but the signal by only a factor of 3. As a result, both cases yield similar sensitivity bounds for the Higgs boson self-coupling λ. However, we note that the higher event rate with one b tag will provide better control of experimental systematic uncertainties, so this may be the preferred strategy.

In addition to the backgrounds considered so far, $b\bar{b}\gamma\gamma$ events (or their fakes) may also be produced in double parton scattering (DPS), or from multiple interactions occurring from separate pp collisions in the same bunch crossing at high luminosity running. In principle, one can identify multiple interactions by a total visible energy measurement or by tracing some final particle tracks back to distinct event vertices, but this may not always be possible in practice. For example, for $b\bar{b}\gamma\gamma$ events where the photon and $b\bar{b}$ pairs occur in different interactions, the latter method relies solely on tracks of particles associated with the hadronic activity

accompanying the photon pair. If these particles are soft, the two vertices may not be clearly resolvable.

To estimate the cross sections from DPS and multiple interactions, we use the approximation outlined in Ref. [41]. In both cases, the dominant contribution arises from multijet production where several jets are misidentified as b quarks or photons. After applying the cuts listed in Eqs. (3) and (4), the DPS and multiple interaction backgrounds are still several times larger than the signal. However, to discriminate them from regular single interaction events, one can exploit the independence and pairwise momentum balance of the two scatterings in DPS or multiple interaction events, similar to the strategy employed in the DPS analysis carried out by the CDF Collaboration [42]. Rejecting events where two sets of transverse momenta independently add up to a value close to zero will obviously strongly suppress the DPS and multiple interaction background. The signal, on the other hand, is only minimally affected by such a cut. Requiring that events which pass the cuts listed in Eqs. (3) and (4) do not satisfy either

$$|\vec{\mathbf{p}}_T(b)+\vec{\mathbf{p}}_T(\gamma_1)|<20 \text{ GeV}$$

and

$$|\vec{\mathbf{p}}_T(\bar{b})+\vec{\mathbf{p}}_T(\gamma_2)|<20 \text{ GeV} \tag{5}$$

or

$$|\vec{\mathbf{p}}_T(\bar{b})+\vec{\mathbf{p}}_T(\gamma_1)|<20 \text{ GeV}$$

and

$$|\vec{\mathbf{p}}_T(b)+\vec{\mathbf{p}}_T(\gamma_2)|<20 \text{ GeV} \tag{6}$$

totally eliminates the DPS and multiple scattering backgrounds (within the limits of our ability to simulate detector effects), but reduces the signal cross section by about 7%. This has essentially no influence on the Higgs boson self-coupling sensitivity bounds.

Extracting the Higgs boson self-coupling follows the same path as for the $4W$ final state used for larger Higgs masses [20]. To discriminate between signal and background, we use the visible invariant mass m_{vis}, which for this final state is the invariant mass of the Higgs boson pair, corrected for energy loss of the b jets. We show this in Fig. 3 for $m_H=120$ GeV at the LHC, and in Figs. 4 and 5 for $m_H=120$ GeV and $m_H=140$ GeV at the SLHC and VLHC. We do not show the $m_H=140$ GeV case for the LHC, since we expect only about two signal events for an integrated luminosity of 600 fb^{-1}. Figures 3–5 show that the background distribution peaks close to the threshold, whereas the signal distribution reaches its maximum at a somewhat higher value. This is due to the destructive interference between the triangle and box diagrams contributing to $gg\to HH$. It is responsible for an increase in the signal cross section and a shift in the m_{vis} peak position toward lower values, if we assume $\lambda<\lambda_{SM}$, and vice versa. The shape of the visible invariant mass distribution thus helps to discriminate signal and background and to probe the Higgs boson self-coupling

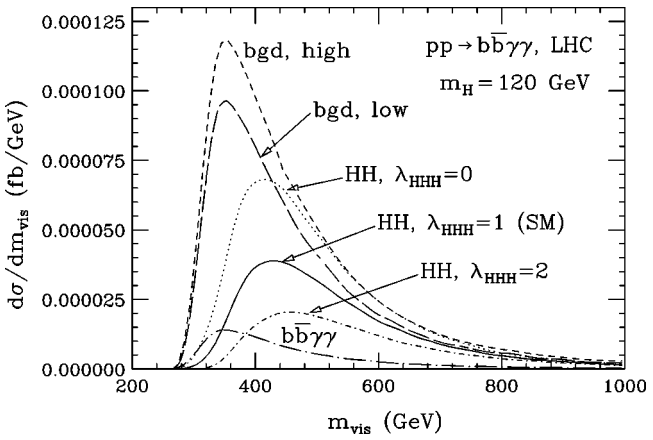

FIG. 3. The visible invariant mass distribution, m_{vis}, in $pp\to b\bar{b}\gamma\gamma$, after all kinematic cuts [Eqs. (3) and (4)], for the conservative (short dashed) and optimistic (long dashed) QCD backgrounds and a SM signal of $m_H=120$ GeV (solid) at the LHC. The dotted and short dash-dotted lines show the signal cross section for $\lambda_{HHH}=\lambda/\lambda_{SM}=0$ and 2, respectively. To illustrate how the reducible backgrounds dominate the analysis, we also show the irreducible QCD $b\bar{b}\gamma\gamma$ background by itself (long dash-dotted). We include the NLO K factor for the signal and a factor of 1.3 for the QCD backgrounds.

λ. Increasing m_H from 120 GeV to 140 GeV reduces the signal (background) cross section by about a factor of 3 (2).

To derive quantitative sensitivity bounds on λ we perform a χ^2 test of the m_{vis} distribution, similar to that described in Ref. [20]. Except for the Higgs boson self-coupling, we assume the SM to be valid. As in all previous analyses, we multiply the LO differential cross sections of the QCD background processes by a factor of 1.3. As mentioned before, this is not a guess at the higher order corrections, which must either be computed, or the rates measured sufficiently precisely. However, in this way we ensure that our results do not critically depend on the absolute normalization of the background rates, while of course they will depend on the uncertainty associated with the determination of the background rate: we allow for a normalization uncertainty of 10% for the SM signal plus background rate. We express limits on the deviation of the Higgs boson self-coupling from the SM value in terms of $\Delta\lambda_{HHH}$, where

$$\Delta\lambda_{HHH}=\lambda_{HHH}-1=\frac{\lambda}{\lambda_{SM}}-1. \tag{7}$$

We summarize our results in Table IV. The bounds obtained using the conservative background estimate (labeled ''hi'') are 10–20 % less stringent than those found using the more optimistic scenario (labeled ''lo''). At the SLHC, for $m_H=120$ GeV, a vanishing Higgs boson self-coupling can be ruled out at the 90% C.L. Limits for $m_H=140$ GeV are a factor of 1.2–2 weaker than those for $m_H=120$ GeV.

It may be possible to subtract large parts of the reducible backgrounds which do not involve charm quarks using the following technique. Due to their large cross sections (see Tables II and III), one can fairly accurately determine the

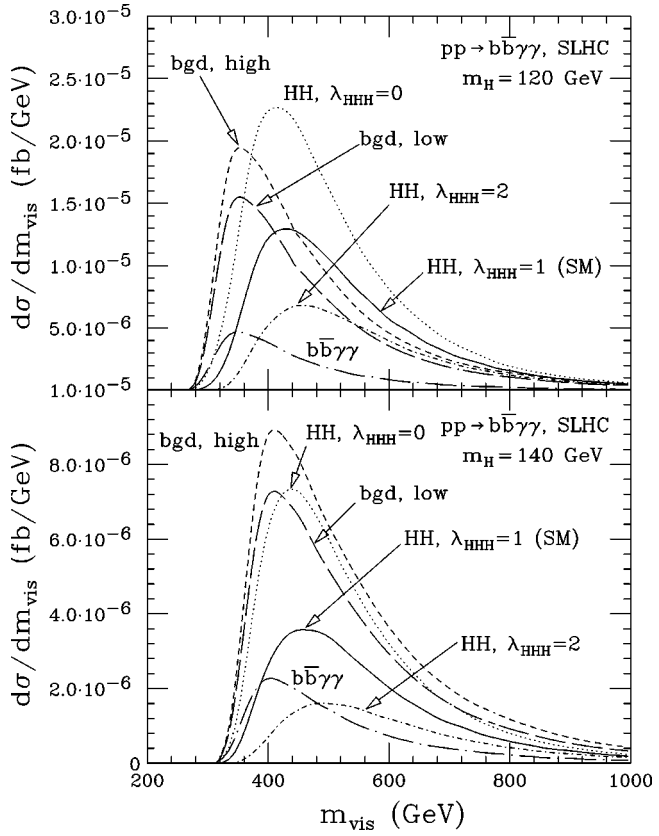

FIG. 4. The visible invariant mass distribution, $m_{\rm vis}$, in $pp \to b\bar{b}\gamma\gamma$, after all kinematic cuts [Eqs. (3) and (4)], for the conservative (short dashed) and optimistic (long dashed) QCD backgrounds and SM signals of $m_H = 120$ (upper) and 140 GeV (lower) at the SLHC. The dotted and short dash-dotted lines show the signal cross section for $\lambda_{HHH} = \lambda/\lambda_{SM} = 0$ and 2, respectively. To illustrate how the reducible backgrounds dominate the analysis, we also show the irreducible QCD $b\bar{b}\gamma\gamma$ background by itself (long dash-dotted). We include the NLO K factor for the signal and a factor of 1.3 for the QCD backgrounds.

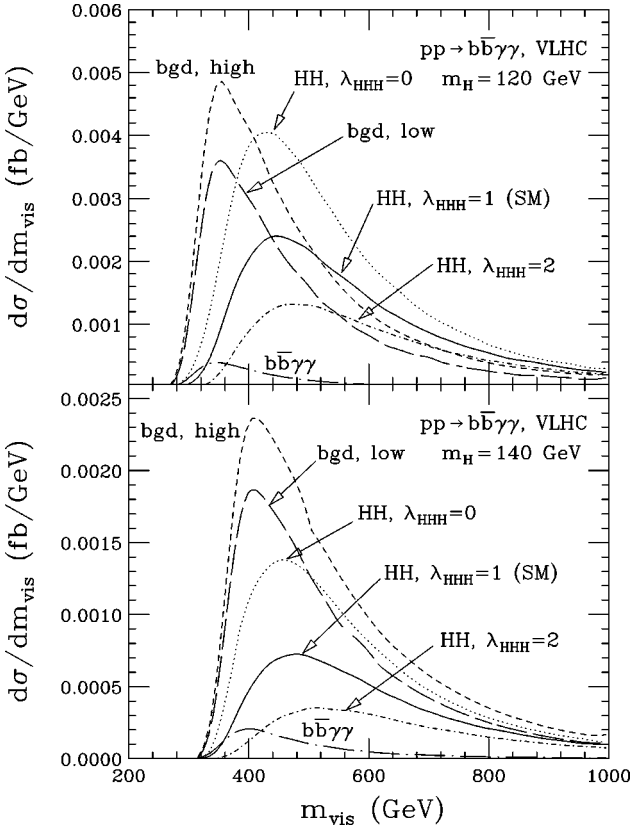

FIG. 5. The visible invariant mass distribution, $m_{\rm vis}$, in $pp \to b\bar{b}\gamma\gamma$, after all kinematic cuts [Eqs. (3) and (4)], for the conservative (short dashed) and optimistic (long dashed) QCD backgrounds and SM signals of $m_H = 120$ (upper) and 140 GeV (lower) at a VLHC. The dotted and short dash-dotted lines show the signal cross section for $\lambda_{HHH} = \lambda/\lambda_{SM} = 0$ and 2, respectively. To illustrate how the reducible backgrounds dominate the analysis, we also show the irreducible QCD $b\bar{b}\gamma\gamma$ background by itself (long dash-dotted). We include the NLO K factor for the signal and a factor of 1.3 for the QCD backgrounds.

$m_{\rm vis}$ distributions of the individual processes, Hjj, $b\bar{b}\gamma j$, $b\bar{b}jj$, $jj\gamma\gamma$, γjjj, and $jjjj$ production, imposing the same cuts as in the $HH \to b\bar{b}\gamma\gamma$ analysis [Eqs. (3) and (4)]. If the photon-jet and light jet-b misidentification probabilities are independently measured in other processes such as prompt photon [43] and $W+$ jets production, one can simply subtract these backgrounds. For the background processes involving charm quarks, on the other hand, this procedure will be more difficult to realize, since the smaller charm quark mass and the shorter charm lifetime result in a charm quark tagging efficiency much lower than that for b quarks. The columns labeled ''Background subtraction'' list the limits achievable if the noncharm reducible contributions to the background were subtracted with 100% efficiency, but none of the charm quark backgrounds could be reduced. Our results show that reducing the background beyond what can be achieved with kinematic cuts may considerably improve the bounds on λ_{HHH} at the LHC and SLHC, where the $HH \to b\bar{b}\gamma\gamma$ process is statistics limited. The bounds achievable at the SLHC (VLHC) by analyzing $b\bar{b}\gamma\gamma$ production are a factor of 2.5–6 (2–3) more stringent than those from the $b\bar{b}\tau^+\tau^-$ channel [22].

Due to the small number of events, the LHC and SLHC sensitivity limits depend significantly on the SM cross section normalization uncertainty. For example, for a normalization uncertainty of 30% on the SM signal plus background rate, the achievable bounds on λ_{HHH} are almost a factor of 2 weaker than those obtained for a normalization uncertainty of 10%. This SM cross section normalization uncertainty depends critically on knowledge of the QCD corrections to the signal and the ability to determine the background normalization. The NLO QCD corrections to $gg \to HH$ are currently known only in the infinite top quark mass limit [36]. To ensure the 10% required precision on differential cross sections we would need the NLO rates for finite top quark masses, as well as the NNLO corrections in the heavy top quark mass limit. For the background normalization one can rely on either calculations of the QCD corrections or data. As

TABLE IV. Expected Higgs boson self-coupling 68.3% C.L. (1σ) sensitivity limits, expressed as $\Delta\lambda_{HHH}=\lambda/\lambda_{SM}-1$, for the various hadron collider options and background analyses presented in the text. There are not enough events at the LHC for $m_H=140$ GeV to perform a measurement of λ. The LHC and VLHC analyses employ a single b tag strategy, while the high luminosity conditions at the SLHC force a double b tag requirement.

Machine	$m_H=120$ GeV			$m_H=140$ GeV		
	"Hi"	"Lo"	Background subtracted	"Hi"	"Lo"	Background subtracted
LHC, 600 fb^{-1}	$+1.9$	$+1.6$	$+0.94$	–	–	–
	-1.1	-1.1	-0.74	–	–	–
SLHC, 6000 fb^{-1}	$+0.82$	$+0.74$	$+0.52$	$+1.7$	$+1.4$	$+0.76$
	-0.66	-0.62	-0.46	-0.9	-0.8	-0.58
VLHC, 600 fb^{-1}	$+0.44$	$+0.42$	$+0.32$	$+0.82$	$+0.66$	$+0.38$
	-0.42	-0.40	-0.30	-0.62	-0.54	-0.34
VLHC, 1200 fb^{-1}	$+0.32$	$+0.30$	$+0.26$	$+0.76$	$+0.62$	$+0.36$
	-0.30	-0.28	-0.22	-0.58	-0.50	-0.32

mentioned before, none of these NLO background calculations are available. Since there are many processes contributing to the background, and most of them involve hundreds of Feynman diagrams already at the tree level, NLO calculations appear feasible only if automated one-loop QCD tools become available in the next few years. In the absence of such NLO results, one may be able to fix the background normalization instead by relaxing the $b\bar{b}$ and $\gamma\gamma$ invariant mass cuts of Eq. (3) and/or the cuts of Eq. (4) and extrapolating from regions in $m_{b\bar{b}}$, $m_{\gamma\gamma}$, $\Delta R(\gamma,b)_{\min}$, and $\Delta R(\gamma,\gamma)$ where the background dominates, back into the analysis region. This technique should make it possible to determine the background normalization to about 10% at the LHC and SLHC, and to about 2% at the VLHC. Both methods rely on Monte Carlo simulation to correctly predict the $m_{\rm vis}$ distribution shape.

The bounds listed in Table IV should be compared with those achievable at e^+e^- linear colliders. A linear collider with $\sqrt{s}=500$ GeV and an integrated luminosity of 1 ab^{-1} can determine λ with a precision of about 20% in $e^+e^-\to ZHH$ for $m_H=120$ GeV [18]. For $m_H>120$ GeV, the $H\to b\bar{b}$ branching ratio and the $e^+e^-\to ZHH$ cross section both fall off quickly. Since the background cross section decreases only slightly, S/B, and thus the bounds on λ obtainable from $e^+e^-\to ZHH$, worsen rapidly with increasing values of m_H. By $m_H=140$ GeV they are at only the 50% level [22]. From Table IV it is clear that the LHC will be able to provide only a first rough measurement of the Higgs boson self-coupling for $m_H=120$ GeV. A luminosity-upgraded LHC will be able to make a more precise measurement. However, the sensitivity bounds on λ obtained from $b\bar{b}\gamma\gamma$ production for $m_H=120$ GeV ($m_H=140$ GeV) will be a factor of 2–4 (1.2–3) weaker than those achievable at a linear collider. In contrast, the sensitivity at a VLHC will approach this level of precision. It should be noted that, if the SM cross section normalization uncertainty could be reduced to a few percent, a VLHC could reach precision similar to that, foreseen for CLIC [17] (e^+e^- collisions at 3 TeV center-of-mass energy).

B. The $b\bar{b}\mu^+\mu^-$ decay channel

The $b\bar{b}\mu^+\mu^-$ signal calculation proceeds as in the $b\bar{b}\gamma\gamma$ case. The basic kinematic acceptance cuts for events at the LHC and VLHC are

$$p_T(b)>45\ \text{GeV},\quad |\eta(b)|<2.5,\quad \Delta R(b,b)>0.4,$$

$$m_H-20\ \text{GeV}<m_{b\bar{b}}<m_H+20\ \text{GeV},$$

$$p_T(\mu)>15\ \text{GeV},\quad |\eta(\mu)|<2.4,\quad \Delta R(\mu,\mu)>0.4,$$

$$m_H-5\ \text{GeV}<m_{\mu\mu}<m_H+5\ \text{GeV},$$

$$\Delta R(b,\mu)>0.4, \tag{8}$$

where again the muon invariant mass window is chosen to accept 79% of the $H\to\mu^+\mu^-$ decay after detector effects. The signal cross section at the LHC (VLHC) for $m_H=120$ GeV before taking into account any efficiencies is 2.4 ab (0.21 fb), approximately one order of magnitude smaller than the $b\bar{b}\gamma\gamma$ channel. For larger Higgs boson masses the ratio is even smaller, due to the $H\to\mu^+\mu^-$ branching ratio, which decreases much more rapidly with m_H than that for $H\to\gamma\gamma$ (see Fig. 1). Once efficiencies are taken into account, we expect less than one signal event at the LHC. The SLHC would see 2–3 signal events for $m_H=120$ GeV if one assumes that both b quarks are tagged, too few for a meaningful coupling extraction. At a VLHC there would be about 60 signal events for an integrated luminosity of 600 fb^{-1}, single b tag requirement, and the same value of m_H. We therefore concentrate on the VLHC in the following, and require only one b tag.

A potential advantage of the $b\bar{b}\mu^+\mu^-$ final state is the smaller number of processes contributing to the background. The main contributions to the background originate from QCD $b\bar{b}\mu^+\mu^-$, $c\bar{c}\mu^+\mu^-$, and $jj\mu^+\mu^-$ production, where the $\mu^+\mu^-$ pair originates from an off-shell Z boson or photon. In the latter two processes, either a charm quark or a light jet is misidentified as a b quark. We calculate the back-

ground processes at LO using MCFM [44] and find that their sum is more than a factor of 200 larger than the signal. The signal-to-background ratio improves by a factor of 5 if we additionally require

$$\Delta R(\mu,\mu)<2, \tag{9}$$

whereas the signal cross section falls by only about 20%. The Hjj background is negligible compared with $jj\mu^+\mu^-$. The final signal to background ratio of $S/B\approx 1/50$ contrasts starkly with the $S/B\sim 1/1$ ratio the $b\bar{b}\gamma\gamma$ channel enjoys. If instead both b jets are tagged, the signal-to-background ratio improves by an additional factor of 2. However, the signal cross section is reduced by a factor of 3, which yields sensitivity bounds for λ_{HHH} that are somewhat weaker than those obtained from single b tag data.

Shrinking the $\mu^+\mu^-$ invariant mass window could also reduce the background. The value in Eq. (8) was chosen assuming ATLAS detector muon momentum resolution [4]. The CMS detector [5] likely can use a smaller window, $|m_H-m_{\mu\mu}|<3$ GeV, which would reduce the background by approximately a factor of 1.7.

The small signal cross section combined with the very large background make it essentially impossible to determine the Higgs boson self-coupling in $pp\to b\bar{b}\mu^+\mu^-$. We quantify this by performing a χ^2 test on the $m_{\rm vis}$ distribution, similar to that described in Sec. III A. Since the signal cross section is too small to be observable at the LHC and SLHC, we derive bounds only for a VLHC. As before, we include the effects of NLO QCD corrections via multiplicative factors: $K=1.35$ for the signal [36], $K=0.81$ for $b\bar{b}\mu^+\mu^-$ and $c\bar{c}\mu^+\mu^-$ production, and $K=0.91$ for the $jj\mu^+\mu^-$ background [44]. Allowing for a normalization uncertainty of 10% of the SM cross sections, for $m_H=120$ GeV we find 1σ bounds of

$$-3.0<\Delta\lambda_{HHH}<4.2 \tag{10}$$

at the VLHC for an integrated luminosity of 600 fb^{-1}. If the $jj\mu^+\mu^-$ background can be subtracted as described in Sec. III A, the limits improve by about a factor of 1.4. Using the CMS dimuon mass window instead, the bound improves by about a factor of 1.3. Nevertheless, this is about an order of magnitude weaker than the limits from $HH\to b\bar{b}\gamma\gamma$.

IV. SUPERSYMMETRIC HIGGS BOSONS

The MSSM requires two Higgs doublets, in contrast to one in the SM, to give mass to the up-type and down-type fermions and to avoid anomalies induced by the supersymmetric fermionic partners of the Higgs bosons. This results in the presence of five physical Higgs bosons: a charged pair $H^\pm$, two neutral scalars h^0 and H^0, and a pseudoscalar A^0. The two scalars are mixed mass eigenstates, the lighter always having a mass $m_h\lesssim 135$ GeV [45]. At leading order, the entire MSSM Higgs sector is described by two parameters, usually taken to be the ratio of the two Higgs doublets' vacuum expectation values, $\tan\beta$, and the pseudoscalar Higgs boson mass m_A. In the region $m_A\gtrsim 150$ GeV, all heavy Higgs bosons $A,H,H^\pm$ have similar masses, much larger than the light scalar Higgs boson mass. In this so-called decoupling regime the light Higgs boson h strongly resembles a SM Higgs boson of the same mass. It will be difficult to distinguish between the SM and the MSSM Higgs sectors through measurements of its properties [3,7].

Assuming bottom-quark–tau mass unification, only two regions of $\tan\beta$ are allowed: either small values, $\tan\beta\lesssim 3$, or large values, $\tan\beta\gtrsim 30$. Direct searches for the heavy Higgs bosons are particularly promising in the large $\tan\beta$ regime, since in the decoupling limit the bottom Yukawa coupling to heavy Higgs bosons is $m_b\tan\beta$. As a result, b-quark-initiated processes, such as $b\bar{b}\to H$, may have cross sections enhanced by up to three orders of magnitude over the corresponding SM rates for sufficiently large values of $\tan\beta$. In contrast, for small values of $\tan\beta$ these direct searches fail, because the dominant Yukawa coupling becomes $m_t/\tan\beta\gg m_b\tan\beta$.

At the LHC, associated production of two neutral MSSM Higgs bosons via gluon fusion occurs for all six possible combinations [29]. In principle, these processes probe the various Higgs boson self-couplings λ_{ijk}. However, for large $\tan\beta$ the continuum box diagrams are enhanced by the Yukawa coupling squared, while the triangle loop diagram with an intermediate Higgs boson is enhanced by only one power of the large Yukawa coupling: for large $\tan\beta$ the resonance diagrams are suppressed by $1/\tan\beta$ as compared to the continuum production diagrams. For $\tan\beta=50$ we find that the effect of vanishing self-couplings $\lambda_{ijk}\equiv 0$ is at maximum at the percentage level.

For $\tan\beta\gtrsim 30$ and $m_A\lesssim 150$ GeV, MSSM Higgs boson pair production cross sections can be sizable, reaching values up to 100 fb, compared to a few tens of femtobarns in the SM. The largest cross sections occur for two heavy states AH, AA, HH and large values of $\tan\beta$, due to the enhanced coupling of these states to b quarks. In this regime the most promising final state is $b\bar{b}\mu^+\mu^-$ since the ratio of the muon and the bottom Yukawa couplings is preserved in the MSSM, but the branching ratio to photons is highly suppressed, typically by several orders of magnitude compared to the SM Higgs boson of equal mass. Unfortunately, a main background for this is MSSM $b\bar{b}H/A,H/A\to\mu^+\mu^-$ production [46]. Whether the Higgs boson pair signal could be extracted out of this would require a more detailed investigation which we do not find likely to be fruitful.

In the small $\tan\beta$ regime it is much more difficult to distinguish the SM and the MSSM Higgs sectors. None of the heavy Higgs bosons will be directly observable at the LHC for $\tan\beta\lesssim 20$, if we rely on the usual decays to fermions. We find that, for small values of $\tan\beta$, $gg\to H\to hh$ offers the best chance to detect the heavy scalar Higgs boson H: for $\tan\beta\lesssim 5$ the $H\to hh$ branching ratio is sizable [50]. To take into account off-shell effects we compute the full $pp\to hh$ production rate. As in the SM, we expect the $b\bar{b}\gamma\gamma$ final state to be most promising in the decoupling regime, with increased rate due to the intermediate H resonance. We show the $h\to b\bar{b}$ and $h\to\gamma\gamma$ branching fractions and lowest

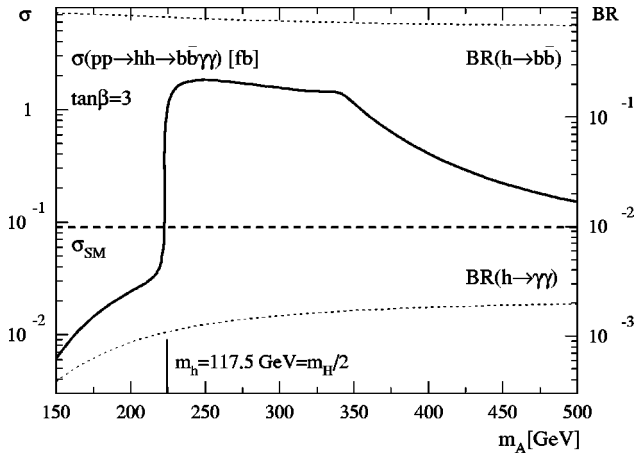

FIG. 6. Lowest order cross section and branching fractions for pair production of light MSSM scalar Higgs bosons, $pp \to hh$, with subsequent decay $hh \to b\bar{b}\gamma\gamma$, as a function of the pseudoscalar Higgs boson mass m_A. We fix $\tan\beta = 3$, set the squark mass parameters to 1 TeV, and assume maximal mixing with $A_t = 2.5$ TeV [47]. We do not take into account supersymmetric decay modes of the heavy Higgs boson H [48]. The light Higgs boson mass is above the LEP limit of $m_H > 114.4$ GeV [49] for $m_A > 190$ GeV. No cuts or detection efficiencies are included. The dashed horizontal line shows the lowest order SM $gg \to HH$ cross section for $m_H = 120$ GeV.

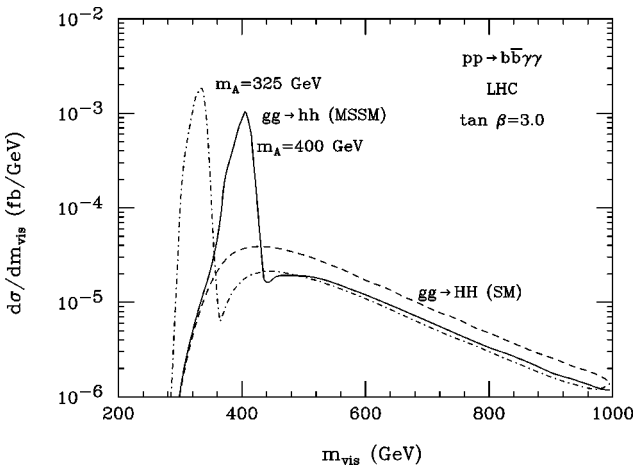

FIG. 7. The visible invariant mass distribution, $m_{\rm vis}$, for MSSM light scalar Higgs boson pair production at the LHC, $pp \to hh \to b\bar{b}\gamma\gamma$, for $\tan\beta = 3$. The light Higgs boson mass for $m_A = 325$ GeV is 120.8 GeV and for $m_A = 400$ GeV it is 122.2 GeV. For comparison, we also show the distribution for SM Higgs boson pair production ($m_H = 120$ GeV).

order $gg \to hh \to b\bar{b}\gamma\gamma$ cross section as a function of m_A in Fig. 6. The light Higgs boson mass increases from $m_h = 108$ GeV for $m_A = 150$ GeV to a plateau value of $m_h = 122$ GeV in the large m_A limit. A few structures in the cross section plot require further explanation. First, the heavy scalar Higgs boson mass crosses the threshold $m_H > 2m_h$ around $m_A \sim 225$ GeV, which enhances the hh cross section by almost a factor of 100. Second, the kink at $m_A \sim m_H = 350$ GeV represents the top threshold in the top triangle loop. At the same time we see the onset of the $H \to t\bar{t}$ decay channel, which for larger values of m_A dominates over $H \to hh$, so the cross section decreases rapidly. Nevertheless, the MSSM signal rate is still enhanced over the SM rate $\sigma_{SM}(b\bar{b}\gamma\gamma) \approx 0.09$ fb for values of m_A as large as 500 GeV.

Unfortunately, the angular cuts of Eq. (4), which are needed to suppress the background, together with the standard $b\bar{b}\gamma\gamma$ identification cuts of Eq. (3), force the differential cross section to vanish for $m_{\rm vis} \lesssim 250$ GeV. Pair production of light supersymmetric Higgs bosons will thus be unobservable for $m_A < 280$ GeV. When taking into account detection efficiencies, we find that hh production at the LHC should be observable at the 5σ level for $320 < m_A < 375$ GeV ($310 < m_A < 425$ GeV) for an integrated luminosity of 300 fb^{-1} (600 fb^{-1}) and $\tan\beta = 3$ [4]. The signal would be rather spectacular: due to s-channel H exchange, the differential cross section peaks for $m_{\rm vis} \approx m_H$, as shown in Fig. 7. Compared to the SM case the cross section is enhanced by more than an order of magnitude in the resonance region, where it depends on the Hhh and $Hf\bar{f}$ couplings. Since MSSM heavy scalar H production with decay into fermions is unobservable at the LHC in the small $\tan\beta$ region, this implies that hh production can measure only a combination of λ_{Hhh} and the $Hf\bar{f}$ couplings, but not the individual couplings.

V. DISCUSSION AND CONCLUSIONS

After discovery of an elementary Higgs boson and tests of its fermionic and gauge boson couplings, experimental evidence that the shape of the Higgs potential has the form required for electroweak symmetry breaking will complete the proof that fermion and weak boson masses are generated by spontaneous symmetry breaking. One must determine the Higgs boson self-coupling to probe the shape of the Higgs potential.

Only Higgs boson pair production at colliders can accomplish this. Numerous studies [15–18] have established that future e^+e^- machines can measure λ at the 20–50 % level for $m_H < 140$ GeV. Very recent studies [19–21] determined that the prospects at hadron colliders for $150 < m_H < 200$ GeV are similarly positive, but that the $m_H < 140$ GeV region would be very difficult to access [22]. We have tried to rectify the situation in this paper by considering highly efficient, lower background rare decay modes: $b\bar{b}\gamma\gamma$ and $b\bar{b}\mu^+\mu^-$. The latter suffers from a very low rate and considerable background from the Breit-Wigner tail of $b\bar{b}Z$ production, and does not appear to be useful. This is not surprising upon comparison to our $b\bar{b}\tau^+\tau^-$ study [22].

However, the $b\bar{b}\gamma\gamma$ channel shows considerable promise. Imposing photon-photon and photon-b separation cuts could result in a signal-to-background ratio of $\mathcal{O}(1)$ or better. Since the irreducible QCD $b\bar{b}\gamma\gamma$ background is small compared to the reducible background originating from light jets or charm quarks mistagged as b quarks, or from jets misidentified as photons, the signal-to-background ratio depends

on the particle misidentification probabilities and the required number of b tags.

We find that the LHC, with an integrated luminosity of 600 fb^{-1} or more, could make a very rough first measurement for $m_H=120$ GeV (with ~ 6 signal events), but would not obtain useful limits for $m_H=140$ GeV at all due to the lack of signal events. It would require a luminosity-upgraded run (SLHC, 6000 fb^{-1}) to rule out $\lambda=0$ at the 90% C.L. for $m_H=120$ GeV, and to make a 50–80 % measurement at the 1σ level. A 200 TeV VLHC, in contrast, would make possible a 20–40 % measurement of λ, competitive with future e^+e^- collider capabilities. We note, however, that current understanding of hadron collider Higgs boson phenomenology does not provide for the necessary precise knowledge of Higgs boson branching ratios to complement this. It is likely that an e^+e^- collider would still be required to fill this role. Although a luminosity-upgraded LHC cannot compete with a linear collider for Higgs boson masses $m_H<140$ GeV, a Higgs boson self-coupling measurement at the SLHC will still be interesting if realized before a linear collider begins operation.

To fully exploit future hadron collider potential to measure the Higgs boson self-coupling, we need an accurate prediction of the SM $b\bar{b}\gamma\gamma$ rate. It is mandatory that the residual theoretical cross section uncertainty be reduced to the 10–15 % level for any HH analysis to be meaningful. We will need similar precision on background rates probably from experiment by extrapolating from background-dominated phase space regions to that of the signal.

Probably the most exciting result of this analysis is the MSSM case: the heavy MSSM Higgs scalar can decay into two light Higgs bosons if $\tan\beta \lesssim 5$. This region of parameter space poses a serious challenge to the LHC, because none of the usual heavy Higgs boson searches will detect a hint of the two Higgs doublets required in the MSSM. Resonant production of the heavy scalar Higgs boson in gluon fusion and its subsequent decay into light Higgs bosons, which then decay to $b\bar{b}\gamma\gamma$, has two effects on the cross section as compared to the SM case: the total rate is enhanced by about an order of magnitude and the hh invariant mass peaks at the heavy Higgs boson mass. Even though our analysis is not at all optimized for resonant MSSM production, we find a 5σ discovery region for $\tan\beta=3$, and $310<m_A<425$ GeV at the LHC. Even though the discovery reach of this channel does not extend to much larger values of $\tan\beta$, it still ensures the observation of one heavy Higgs boson in a region preferred by bottom-quark–tau unification, inaccessible by other MSSM Higgs boson searches.

ACKNOWLEDGMENT

We would like to thank K. Bloom, M. Dührssen, F. Maltoni, B. Mellado, A. Nikitenko, J. Parsons, D. Wackeroth, D. Zeppenfeld, and P. M. Zerwas for useful discussions. We also thank C. Oleari for providing us with the code to calculate the *Hjj* background. One of us (U.B.) would like to thank the Fermilab Theory Group, where part of this work was carried out, for its generous hospitality. This research was supported in part by the National Science Foundation under Grant No. PHY-0139953.

[1] LEPEWWG Collaboration, D. Abbaneo *et al.*, hep-ex/0312023; G. Quast, talk given at the HEP2003 Europhysics Conference, Aachen, Germany, 2003.

[2] M. Dittmar and H.K. Dreiner, Phys. Rev. D **55**, 167 (1997); D. Rainwater and D. Zeppenfeld, *ibid.* **60**, 113004 (1999); **61**, 099901(E) (2000); N. Kauer, T. Plehn, D. Rainwater, and D. Zeppenfeld, Phys. Lett. B **503**, 113 (2001); N. Akchurin *et al.*, Report No. CMS-NOTE-2002/066; B. Mellado, Report No. ATL-CONF-2002-004.

[3] S. Asai *et al.*, Report No. ATL-PHYS-2003-005; G. Azuelos and R. Mazini, Report No. ATL-PHYS-2003-004; M. Dührssen, Report No. ATL-PHYS-2003-010.

[4] ATLAS TDR Collaboration, Report No. CERN/LHCC/99-15, 1999.

[5] CMS TP Collaboration, Report No. CERN/LHCC/94-38, 1994.

[6] D. Rainwater, D. Zeppenfeld, and K. Hagiwara, Phys. Rev. D **59**, 014037 (1999); T. Plehn, D. Rainwater, and D. Zeppenfeld, Phys. Lett. B **454**, 297 (1999); Phys. Rev. D **61**, 093005 (2000).

[7] D. Zeppenfeld, R. Kinnunen, A. Nikitenko, and E. Richter-Was, Phys. Rev. D **62**, 013009 (2000); M. Hohlfeld, Report No. ATL-PHYS-2001-004.

[8] D. Rainwater, Phys. Lett. B **503**, 320 (2001); V. Drollinger, T. Müller, and D. Denegri, hep-ph/0201249.

[9] V. Drollinger, T. Müller, and D. Denegri, hep-ph/0111312; V. Kostioukhine, J. Leveque, A. Rozanov, and J.B. de Vivie, Report No. ATL-PHYS-2002-019; D. Green *et al.*, Report No. FERMILAB-FN-705, 2001; F. Maltoni, D. Rainwater, and S. Willenbrock, Phys. Rev. D **66**, 034022 (2002); A. Belyaev and L. Reina, J. High Energy Phys. **08**, 041 (2002); A. Belyaev, F. Maltoni, and L. Reina, in Proceedings of the APS/DPF/DPB Summer Study on the Future of Particle Physics (Snowmass 2001), edited by N. Graf, hep-ph/0110274.

[10] O.J. Éboli and D. Zeppenfeld, Phys. Lett. B **495**, 147 (2000).

[11] T. Plehn and D. Rainwater, Phys. Lett. B **520**, 108 (2001); T. Han and B. McElrath, *ibid.* **528**, 81 (2002).

[12] ECFA/DESY LC Physics Working Group Collaboration, J.A. Aguilar-Saavedra *et al.*, hep-ph/0106315, and references therein; American Linear Collider Working Group Collaboration, T. Abe *et al.*, in Proceedings of the APS/DPF/DPB Summer Study on the Future of Particle Physics (Snowmass 2001), edited by R. Davidson and C. Quigg, hep-ex/0106056, and references therein.

[13] B.W. Lee, C. Quigg, and H.B. Thacker, Phys. Rev. Lett. **38**, 883 (1977); Phys. Rev. D **16**, 1519 (1977).

[14] D.A. Dicus, C. Kao, and S.S. Willenbrock, Phys. Lett. B **203**, 457 (1988); E.W. Glover and J.J. van der Bij, Nucl. Phys. **B309**, 282 (1988); E. W. Glover and J. J. van der Bij, in Proceedings of the 23rd Rencontres de Moriond: Current Issues in

Hadron Physics, Les Arcs, France, 1988, Report No. CERN-TH-5022-88; G. Cynolter, E. Lendvai, and G. Pocsik, Acta Phys. Pol. B **31**, 1749 (2000).
[15] F. Boudjema and E. Chopin, Z. Phys. C **73**, 85 (1996); V.A. Ilyin *et al.*, Phys. Rev. D **54**, 6717 (1996).
[16] A. Djouadi, W. Kilian, M. Mühlleitner, and P.M. Zerwas, Eur. Phys. J. C **10**, 27 (1999); D.J. Miller and S. Moretti, *ibid.* **13**, 459 (2000).
[17] M. Battaglia, E. Boos, and W.M. Yao, in Proceedings of the APS/DPF/DPB Summer Study on the Future of Particle Physics (Snowmass 2001) [12], hep-ph/0111276.
[18] C. Castanier, P. Gay, P. Lutz, and J. Orloff, hep-ex/0101028.
[19] F. Gianotti *et al.*, hep-ph/0204087.
[20] U. Baur, T. Plehn, and D. Rainwater, Phys. Rev. Lett. **89**, 151801 (2002); Phys. Rev. D **67**, 033003 (2003).
[21] A. Blondel, A. Clark, and F. Mazzucato, Report No. ATL-PHYS-2002-029, 2002.
[22] U. Baur, T. Plehn, and D. Rainwater, Phys. Rev. D **68**, 033001 (2003).
[23] G. Ambrosio *et al.*, Report No. Fermilab-TM-2149, 2001.
[24] S. Kanemura *et al.*, Phys. Lett. B **558**, 157 (2003).
[25] W. Hollik and S. Penaranda, Eur. Phys. J. C **23**, 163 (2002); A. Dobado, M.J. Herrero, W. Hollik, and S. Penaranda, Phys. Rev. D **66**, 095016 (2002).
[26] D.B. Kaplan and H. Georgi, Phys. Lett. **136B**, 183 (1984); H. Georgi, *ibid.* **151B**, 57 (1985).
[27] C. Csaki *et al.*, Phys. Rev. D **68**, 035009 (2003); T. Han, H.E. Logan, B. McElrath, and L.T. Wang, *ibid.* **67**, 095004 (2003); C. Dib, R. Rosenfeld, and A. Zerwekh, hep-ph/0302068.
[28] V. Barger *et al.*, Phys. Rev. D **67**, 115001 (2003).
[29] T. Plehn, M. Spira, and P.M. Zerwas, Nucl. Phys. **B479**, 46 (1996); [**B531**, 655(E) (1998)]; A. Djouadi, W. Kilian, M. Mühlleitner, and P.M. Zerwas, Eur. Phys. J. C **10**, 45 (1999); A.A. Barrientos Bendezu and B.A. Kniehl, Phys. Rev. D **64**, 035006 (2001).
[30] A. Dobrovolskaya and V. Novikov, Z. Phys. C **52**, 427 (1991); D.A. Dicus, K.J. Kallianpur, and S.S. Willenbrock, Phys. Lett. B **200**, 187 (1988); A. Abbasabadi, W.W. Repko, D.A. Dicus, and R. Vega, *ibid.* **213**, 386 (1988); W.Y. Keung, Mod. Phys. Lett. A **2**, 765 (1987).
[31] V.D. Barger, T. Han, and R.J. Phillips, Phys. Rev. D **38**, 2766 (1988).
[32] K. Long, in Proceedings of the 31st International Conference on High Energy Physics, Amsterdam, The Netherlands (to be published), 2002 hep-ex/0212008.
[33] CTEQ Collaboration, H.L. Lai *et al.*, Eur. Phys. J. C **12**, 375 (2000).
[34] A. Nikitenko (private communication).
[35] T. Stelzer and W.F. Long, Comput. Phys. Commun. **81**, 357 (1994); F. Maltoni and T. Stelzer, J. High Energy Phys. **02**, 027 (2003).
[36] S. Dawson, S. Dittmaier, and M. Spira, Phys. Rev. D **58**, 115012 (1998).
[37] R. Hawkings, ATLAS Report No. SN-ATLAS-2003-026.
[38] Ph. Schwemling, ATLAS Report No. SN-ATLAS-2003-034.
[39] S. Abdullin *et al.*, Phys. Lett. B **431**, 410 (1998).
[40] V. Del Duca *et al.*, Nucl. Phys. **B616**, 367 (2001).
[41] V.D. Barger, K.M. Cheung, T. Han, and R.J. Phillips, Phys. Rev. D **42**, 3052 (1990).
[42] CDF Collaboration, F. Abe *et al.*, Phys. Rev. D **56**, 3811 (1997).
[43] CDF Collaboration, F. Abe *et al.*, Phys. Rev. Lett. **74**, 1936 (1995); **74**, 1941 (1995); D0 Collaboration, S. Abachi *et al.*, *ibid.* **78**, 3634 (1997); **75**, 1028 (1995).
[44] J.M. Campbell and R.K. Ellis, Phys. Rev. D **62**, 114012 (2000); J. Campbell, R.K. Ellis, and D. Rainwater, *ibid.* **68**, 094021 (2003).
[45] G. Degrassi *et al.*, Eur. Phys. J. C **28**, 133 (2003).
[46] E. Boos, A. Djouadi, and A. Nikitenko, hep-ph/0307079.
[47] S. Heinemeyer, W. Hollik, and G. Weiglein, Comput. Phys. Commun. **124**, 76 (2000); hep-ph/0002213.
[48] A. Djouadi, J. Kalinowski, and M. Spira, Comput. Phys. Commun. **108**, 56 (1998).
[49] LEP Collaboration, G. Abbiendi *et al.*, Phys. Lett. B **565**, 61 (2003).
[50] R. Lafaye, D.J. Miller, M. Mühlleitner, and S. Moretti, hep-ph/0002238, and Ref. [9] therein.